ACS OMEGA

Article

Cite This: ACS Omega 2018, 3, 8497−8505

http://pubs.acs.org/journal/acsodf

Structure-Driven Discovery of α,γ-Diketoacid Inhibitors Against UL89 Herpesvirus Terminase

Salvatore Bongarzone,[†,‡,#] Marta Nadal,[†,‡,¶] Zuzanna Kaczmarska,[†,‡,▽] Cristina Machón,[†,‡] Mercedes Álvarez,[†,§,∥] Fernando Albericio,[†,§,⊥] and Miquel Coll*[,†,‡]

[†]Institute for Research in Biomedicine (IRB Barcelona), The Barcelona Institute of Science and Technology, Baldiri Reixac 10-12, 08028 Barcelona, Spain

[‡]Molecular Biology Institute of Barcelona (IBMB—CSIC), Barcelona Science Park, Baldiri Reixac 10-12, 08028 Barcelona, Spain

[§]CIBER-BBN, Networking Centre on Bioengineering, Biomaterials and Nanomedicine, Barcelona Science Park, 08028 Barcelona, Spain

[∥]Laboratory of Organic Chemistry, Faculty of Pharmacy, University of Barcelona, 08028 Barcelona, Spain

[⊥]Department of Organic Chemistry, University of Barcelona, Martí i Franquès 1, 08028 Barcelona, Spain

Supporting Information

ABSTRACT: Human cytomegalovirus (HCMV) is an opportunistic pathogen causing a variety of severe viral infections, including irreversible congenital disabilities. Nowadays, HCMV infection is treated by inhibiting the viral DNA polymerase. However, DNA polymerase inhibitors have several drawbacks. An alternative strategy is to use compounds against the packaging machinery or terminase complex, which is essential for viral replication. Our discovery that raltegravir (**1**), a human immunodeficiency virus drug, inhibits the nuclease function of UL89, one of the protein subunits of the complex, prompted us to further develop terminase inhibitors. On the basis of the structure of **1**, a library of diketoacid (α,γ-DKA and β,δ-DKA) derivatives were synthesized and tested for UL89-C nuclease activity. The mode of action of α,γ-DKA derivatives on the UL89 active site was elucidated by using X-ray crystallography, molecular docking, and in vitro experiments. Our studies identified α,γ-DKA derivative **14** able to inhibit UL89 in vitro in the low micromolar range, making **14** an optimal candidate for further development and virus-infected cell assay.

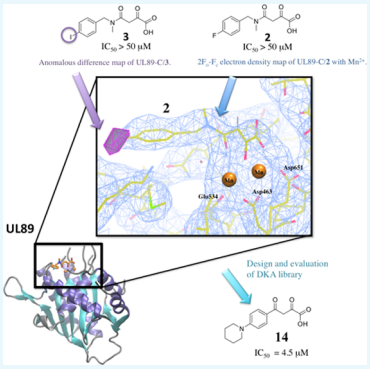

INTRODUCTION

Human cytomegalovirus (HCMV), one of the eight known human herpesviruses, is widespread with a high prevalence throughout the human population.[1] HCMV causes severe diseases and life-threatening conditions in immune-compromised individuals, such as acquired immunodeficiency syndrome, and organ transplant patients, neonates, and young children.[1] It is the leading congenital infection in developed countries, causing a number of neural abnormalities including hearing loss, mental retardation, and microcephalia. The drugs licensed so far for the treatment of HCMV infection are the antisense oligonucleotide fomivirsen and four viral DNA polymerase inhibitors: ganciclovir (GCV), valganciclovir, cidofovir (CDV), and foscarnet (FOS).[2] There are several disadvantages associated with the use of these drugs including (i) poor bioavailability, (ii) serious side effects induced by prolonged treatment, and (iii) emergence of resistant viral strains.[3] Development of drug resistance is associated with an aggressive clinical course, organ dysfunction, and mortality.[4] Several cases of multidrug resistance to GCV, CDV, and FOS have been reported.[5] Therefore, there is an urgent need for the development of new drugs with a different mode of action, good bioavailability, and a safer pharmacological profile. Novel classes of antiviral compounds able to target viral entry, transcription, protein synthesis and processing, genome replication, or maturation have been identified.[2,6−13] Among these, a promising strategy is to block the HCMV terminase machinery[14] which mediates DNA binding, cleavage, and packaging because these processes do not occur in mammalian cells and therefore specific terminase inhibitors could have fewer undesirable side effects.

HCMV replicates its genome as concatamers that are large DNA molecules with several copies of the genome. Afterward, these are cut into single unit-length genome and packaged inside the capsids by the HCMV terminase machinery.[15] HCMV terminase is a protein complex composed of UL56, UL89, and UL51 responsible for binding, cleavage, and translocation of viral DNA inside the procapsids, respectively.[15−17] The three-dimensional (3D) structure of the nuclease domain of UL89 was determined by X-ray crystallography,[18] whereas the structures of UL56 and UL51 are not elucidated yet.

Received: June 27, 2018
Accepted: July 19, 2018
Published: August 1, 2018

DOI: 10.1021/acsomega.8b01472
ACS Omega 2018, 3, 8497−8505

Letermovir, a 3,4-dihydro-quinazoline-4-yl-acetic acid derivative, a non-nucleoside inhibitor with a potent antiviral activity, specific against the viral terminase subunit pUL56,[19,20] has been developed by AiCuris GmbH & Co KG and is currently in a phase III clinical study.[21] An alternative approach consists of targeting UL89, another subunit of the terminase complex, which contains two domains, the C-terminal region (UL89-C, 418-674), which has proved nuclease activity,[16,18,22] and the N-terminal part (UL89-N, 1-417), which has putative adenosine-triphosphatase activity.[23−25] UL89 inhibitors may be designed to block the adenosine 5′-triphosphate (ATP) binding site on the UL89-N region; amongst them, there are 2-bromo-5,6-dichloro-1-β-D-ribofuranosyl benzimidazole (Figure S1), 2,5,6-trichloro-1-(β-D-ribofuranosyl)benzimidazole, 2-bromo-5,6-dichloro-1-β-D-ribopyranosyl-1*H*-benzimidazole (GW275175X), and 3-hydroxy-2,2-dimethyl-*N*-[4([[5-(dimethylamino)-1-naphthyl]sulfonyl]amino)-phenyl]propanamide (BAY 38-4766), which interact with the ATP binding site and induce mutations on the UL89-N domain.[15,26−32] However, in spite of the efforts, none of them have reached the market.[2,6,7] The presence of the highly conserved ATP binding motif in many different proteins could impede to obtain specific inhibitors for the viral UL89-N.[33]

Another approach is focused on finding HCMV inhibitors able to target the nuclease activity of UL89-C. The structure of UL89-C, which is structurally related to the human immunodeficiency virus (HIV) integrase,[18] exhibits a central eight-stranded mixed β-sheet, with parallel and antiparallel strands, flanked on both sides by six α-helices. The nuclease active site of UL89-C is located in a cleft formed by three loops $\beta2-\beta3$, $\beta5-\alpha3$, and $\alpha5-\alpha6$. Three acidic residues Asp463, Asp651, and Glu534 chelate two Mn^{2+} ions, which are essential for UL89-C DNA cleavage. An UL89-C nuclease inhibitor should interact with the two Mn^{2+} ions and the amino acids located in the loops to block DNA interaction and cleavage.

Most of the compounds against UL89-C tested so far are divalent metal-sequestering inhibitors, such as 1-(3-chloro-4-fluorobenzyl)-5-hydroxy-4-oxo-1,4-dihydropyridine-3-carboxylic acid[34] (Figure S1), an hydroxypyridonecarboxylic (HPC) derivative, and 3-hydroxy-1-methyl-6-((4′-methyl-[1,1′-biphenyl]-4-yl)amino)dihydropyrimidine-2,4(1*H*,3*H*)-dione[35] (Figure S1), a 3-hydroxypyrimidine-2,4-dione (HPD) derivative. HPC and HPD compounds inhibit the nuclease activity of UL89-C in the low micromolar range (IC_{50} = 2.2 and 1 μM, respectively), HCMV replication, and infectious virus production in cell culture.[35] Therefore, there is a correlation between blocking of pUL89 endonuclease activity and inhibition of HCMV replication and viral genome cleavage. Recently, 2,7-dihydroxy-4-(propan-2-yl)cyclohepta-2,4,6-trien-1-one (Figure S1) with metal-chelating motifs was identified as an inhibitor of pUL15C of herpes simplex viruses 1, a homologue of pUL89-C.[36] Crystallographic studies of 2,7-dihydroxy-4-(propan-2-yl)cyclohepta-2,4,6-trien-1-one binding to the nuclease active site of bacteriophage terminase gp2 nuclease domain revealed that the interaction is mainly mediated by the two metal ions (PDB code: 5C2F).[37]

Previous studies have reported the structure−activity relationships (SARs) of UL89 inhibitors explained by molecular docking simulation, using the apo form of UL89, without the possibility to validate docking binding mode because there is no UL89-inhibitor complex available. Clearly, it is important to have an understanding of the interactions of UL89 inhibitors with UL89 and offer detailed information to drive a target-based drug discovery program against HCMV. We have focused our efforts on elucidating the 3D structural data of UL89 inhibitors with UL89-C.[18] In our previous report, we found that pUL89-C endonuclease activity was inhibited by the HIV inhibitor raltegravir (**1**, Figure 1), suggesting that inhibiting pUL89-C is possible using a similar metal-chelating pharmacophore.[18]

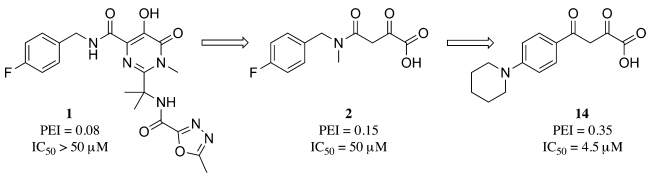

Figure 1. Rational design of **14** as the UL89-C inhibitor.

On the basis of computational molecular docking studies of **1** (Figure S2A), the pivotal chemical regions of **1** binding pUL89-C endonuclease domain active site were identified. Upon definition of the chemical features, a new set of compounds was designed to improve the inhibition activity. Herein, we present the synthesis and evaluation of a library of small organic compounds able to inhibit UL89-C nuclease activity in an in vitro enzymatic assay. The ability of these compounds to bind UL89-C was tested by thermal denaturation. Furthermore, the X-ray structure of a protein−ligand complex unveiled the precise binding mode of the ligand in the enzyme active site, allowing a further structure-driven antiviral development against UL89-C activity.

RESULTS AND DISCUSSION

Rational Design and Chemistry. Our rational design began by simplifying the structure of **1**, a HIV integrase inhibitor, by selecting chemical features important for UL89-C binding. Computational docking studies of **1** in the active site of UL89-C highlighted a number of molecular interactions that contribute to binding affinity (Figure S2A). The pivotal regions of **1** binding the pUL89-C active site are the metal chelator group and the benzyl group. The three coplanar oxygen atoms of the diketo acid (DKA) moiety chelate Mn^{2+} ions in the active site, explaining the requirement for metal ions for drug binding. The central oxygen, O(H), bridges both metal ions, whereas two O (carbonyl) coordinates the metal ions (Figure S2A). Additionally, the terminal phenyl ring interacts with Asn536 (distance = 3.74 Å), Met579 (3.30 Å), and Thr537 (4.66 Å). These interactions could help position the inhibitor near the divalent metal cations in the active site. The five-membered oxadiazole moiety and isopropyl group are not directly involved into interactions with the UL89-C binding site (distance oxadiazole-Phe466 > 6.24 Å).

On this basis, we designed **2** containing an α,γ-DKA motif linked to a 4-fluorophenyl ring (Figures 1 and 2A). The α,γ-DKA core, a privileged structure found in thousands of HIV integrase inhibitors with IC_{50} values in low micromolar concentrations,[38−45] is able to chelate Mn^{2+}[46] (Figure S2A) and able to disrupt DNA−protein interactions.[38,43,45,47−49] The α,γ-DKA motif has also been successfully used as a starting point to obtain inhibitors against (1) hepatitis C virus NS5B polymerase,[50] (2) HIV-reverse transcriptase RNase H,[51] (3) hepatitis C virus NS5b polymerase,[52] and (4) influenza endonuclease.[53] The 4-fluorophenyl ring is a common motif found in **1** and other inhibitors.

DOI: 10.1021/acsomega.8b01472
ACS Omega 2018, 3, 8497−8505

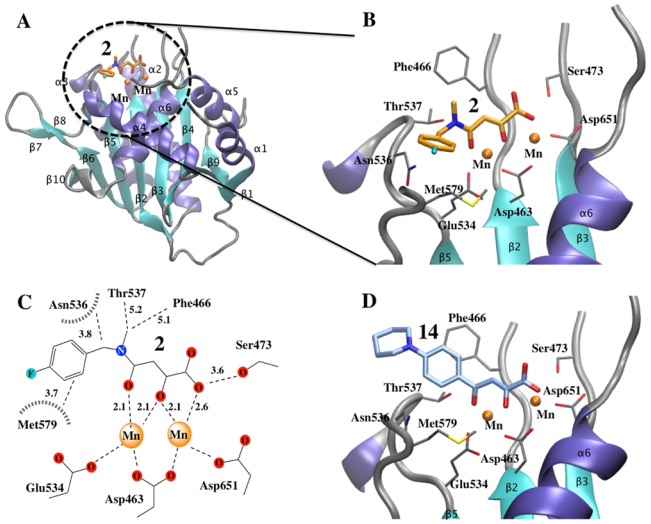

Figure 2. Binding mode of **2** and **14** to UL89-C (A) X-ray crystal structure of **2** (orange, PDB code: 6EY7) bound to UL89-C. Mn^{2+} atoms are shown as orange spheres. (B) Close-up view of the active site in A. (C) Hydrogen-bonding network and hydrophobic interactions between UL89-C, Mn^{2+}, and **2** are depicted (mean distances shown in Angstrom). (D) Docked conformation of **14** (iceblue) in the UL89-C active site.

To validate our binding pose predictions and to facilitate further structural modifications, we determined the crystal structure of UL89-C bound with **2** (PDB code 6EY7). The elucidation of the binding mode of **2** in the UL89-C binding site by X-ray crystallography (see below and Figure 2A) and the finding of **2** able to inhibit UL89-C prompted us to enlarge the α,γ-DKA series (**3**−**17**, Schemes 1 and 2). The substituents on

Scheme 1. Reagents and Conditions: (a) CH_3NH_2 or $C_6H_{11}NH_2$, Tetrahydrofuran (THF), Room Temperature (rt), 12 h (35−40% Yield); (b) 2c−5c, CH_3COCl, NEt_3, CH_2Cl_2, 0 °C, 2 h (82−99%); (c) LiHMDS, THF, −78 °C, 0.5 h, Then $(CH_3OCO)_2$, 0 °C, 4 h (38−95%); (d) LiOH 1 N, MeOH, 40 °C, 2 h (49−100%); and (e) Amine, HBTU, DIEA, Dimethylformamide (DMF), rt, Overnight (26−44%)

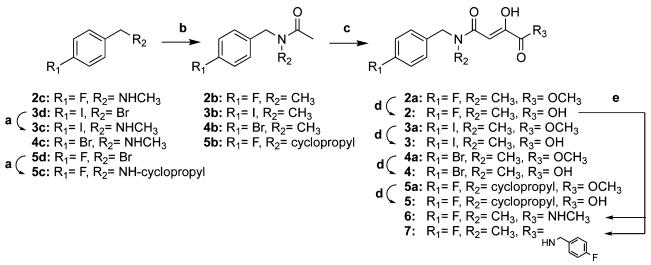

the aromatic ring (**3**−**4**), amide (**5**), carboxylic acid (**6**−**7**), and benzylic (**8**−**17**) positions were studied to determine SAR of the series. The fluoride atom of **2** was substituted with iodine (**3**) and bromine (**4**). In **5**, the methyl group of the amide portion was exchanged for a bulkier alkyl substituent. Furthermore, the carboxylic functionality of **2** was converted to an amide (**6**−**7**). The 4-fluorobenzyl and the *N*-methyl-4-fluorobenzylamine groups of **2** were exchanged with a CH_3 group to give **8** and **9**, respectively. Different planar (hetero)aromatic rings, variously decorated, have been added to the α,γ-DKA chelating

Scheme 2. Reagents and Conditions: (a) LiOH 1 N, MeOH, 40 °C, 1 h (69−79% Yield)

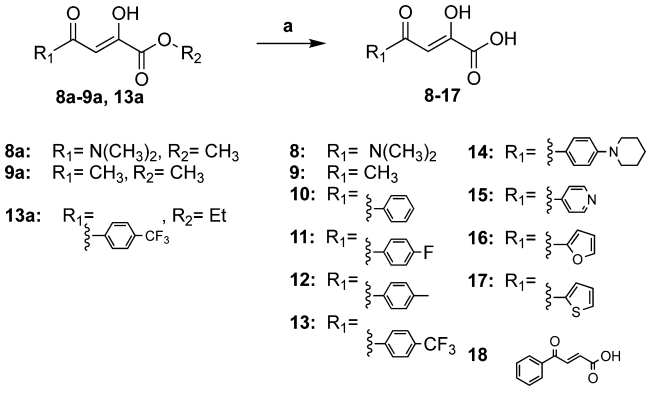

core (**10**−**17**) to promote a $\pi-\pi$ stacking interaction with Phe466.

On the basis of the remarkable profile shown by α,γ-DKA derivatives, **18**, lacking the α,γ-DKA core required to achieve chelation, was used as the negative control. The synthesis of compounds **2**−**5** and **8** was straightforward and was accomplished in three reaction steps. In the first step, the primary amine (**2c**−**5c**, Scheme 1) was acetylated under standard conditions to afford the intermediate **2b**−**5b**. The preparation of intermediates **2a**−**5a** was achieved by treating **2b**−**5b** with dimethyl oxalate. Then, **2a**−**5a** were hydrolyzed to afford the corresponding acid derivatives (**2**−**5**).[44,54,55] Compounds **6** and **7** were obtained by coupling methylamine and 4-fluorobenzylamine, respectively, with **2**. Compounds **8**−**9** and **13** were prepared by basic hydrolysis of **8a**−**9a** and **13a** (Scheme 2).

Finally, on the basis of the structure of a potent HIV integrase inhibitor MK-2048 (Figure S3A), we substituted the α,γ-DKA core with a β,δ-DKA chelating group (**19**−**20** and Figure S3A). The synthesis of **19**−**20** (Scheme 3) started from the formation

Scheme 3. Reagents and Conditions: (a) $HC(OEt)_3$, $CO(NH_2)_2$, Refluxing Xylenes, 4 h (57% Yield); (b) 23, EtBr, K_2CO_3, DMF, 80 °C, 14 h (34%); (c) 22 (1 equiv), KOH (1 equiv), EtOH, rt, Overnight (65%); (d) 21, *N*-(4-Fluorobenzyl)-*N*-metilamine or *N*-4-Fluorobenzylamine, EDCI, HOAt, DCM, rt, Overnight (35−36%); and (e) LiOH 1 N, MeOH, 40 °C, 1 h (43−97%)

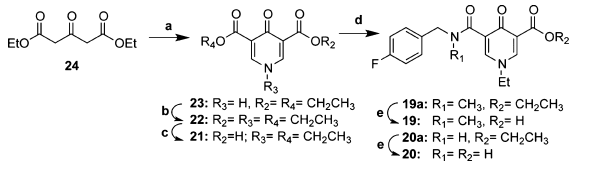

of the dihydropyridone core (**23**), which was subsequently ethylated giving **22** and then partially hydrolyzed obtaining **21**.[56−58] Afterward, **19b** and **20b** were obtained by coupling benzylamines with **21**, using amide coupling reagents. Finally, ester derivatives **19b** and **20b** were converted to **19** and **20**, respectively.

UL89-C/2 Complex Structure. To study the binding mode of **2**, we determined the 3D crystal structure of the UL89-C/**2** complex (PDB code 6EY7). Diffraction data collected from crystals of UL89-C soaked with Mn^{2+} and **2** were solved by molecular replacement, using the solved inhibitor-free UL89-C

DOI: 10.1021/acsomega.8b01472
ACS Omega 2018, 3, 8497−8505

Table 1. In Vitro Activities of 1−20 Against UL89-C

compound	% inhibition at 50.0 μM	% inhibition at 25.0 μM	% inhibition at 12.5 μM	% inhibition at 6.25 μM	% inhibition at 3.12 μM
1	36.6 ± 7.1[a]	22.1 ± 10.6			
2	56.2 ± 4.9	20.3 ± 7.1			
2b	n.a.[b]				
3	47.7 ± 7.1	26.8 ± 7.1			
4	51.5 ± 7.8	10.7 ± 8.5			
5	76.3 ± 4.2	52.2 ± 3.9	22.6 ± 1.4		
6	n.a.				
7	n.a.				
8	n.a.				
9	n.a.				
10	62.6 ± 12.0	46.6 ± 4.2	29.7 ± 3.5		
11	26.8 ± 4.2	3.6 ± 2.8			
12	89.1 ± 5.7	47.6 ± 0.4	32.7 ± 0.7		
13	42.6 ± 6.4	15.4 ± 7.1			
14	97.2 ± 5.0	90.6 ± 3.5	65.0 ± 2.8	45.8 ± 7.1	12.5 ± 2.8
15	75.6 ± 1.4	33.3 ± 14.1	1.1 ± 0.7		
16	66.7 ± 1.4	52.0 ± 3.5	28.2 ± 0.9		
17	96.9 ± 1.4	92.3 ± 6.4	80.0 ± 7.1	24.0 ± 0.7	14 ± 7.1
18	n.a.				
19	n.a.				
20	n.a.				

[a]Mean and SD of three experiment. [b]n.a. = not active.

as the initial model.[18] Strong electron density within the active site was observed adjacent to the Mn^{2+} ions (Figure S2B).

The UL89-C/**2** structure was refined to 2.9 Å resolution (Table 2). The UL89-C/**2** crystal also showed anomalous scattering, confirming the presence of two Mn^{2+} ions in the active site. As expected, **2** bound through the α,γ-DKA core to the two Mn^{2+} ions in the active site (Figure 2B). The three adjacent oxygen atoms of the α,γ-DKA fragment chelated the two Mn^{2+} ions in a pairwise fashion such that the central oxygen atom was bridging the two ions (Figure 2B). Thus, the Mn^{2+} ions were coordinated by two acidic residues (Glu534-Asp463 or Asp463-Asp651) from UL89-C and two oxygen atoms of **2** (Figure 2B) in a tetrahedral geometry. An identical coordination pattern has been observed between the active site of LACV L-protein and an α,γ-DKA derivative.[59] All four compounds in the asymmetric unit of the UL89-C/**2** crystals showed clear electron density for the orientation displayed in Figure 2A. The complex UL89-C/**2** also revealed that the 4-fluorobenzyl group blocks a region crucial for DNA/UL89-C recognition. To further confirm the presence of **2** in the UL89-C/**2** complex, we exchanged the fluorine atom for iodine (**3**) or bromine (**4**) atom because both are able to originate measurable anomalous scattering effects. Indeed, the anomalous difference maps confirmed the presence of the iodine atom of **3** in the UL89-C/**3** complex (Table 2). The position of the iodine atom on the UL89-C/**3** complex overlaps with the fluorine atom of **2** found in UL89-C/**2** (Figure S2C). On the basis of the crystallographic studies on UL89-C/**2** and UL89-C/**3**, the α,γ-DKA chelating core served as the metal-binding motif and the 4-fluorophenyl ring afforded additional interactions with the hydrophobic cleft formed by Asn536 and Met579 (Figure 2B,C). The methyl group of **2**, pointing outside the binding site, may be substituted with a bulky alkyl group to get an additional hydrophobic interaction with the close Phe466 (Figure 2B,C). The carboxylic acid interacted with Ser473 by hydrogen bonds with a distance of 3.6 Å (Figure 2C).

Inhibition of UL89-C Nuclease Activity. A quantitative UL89-C nuclease assay was designed to evaluate the inhibition potency of **1**−**20**. These compounds passed through a pan assay interference compounds filter (http://zinc15.docking.org/patterns/home/).[60]

Linear DNA and UL89-C were incubated at 37 °C for 30 min in the presence of **1**−**20** at a concentration of 50 μM. Linear DNA was run on an agarose gel electrophoresis gel, stained with Syto 60, and quantified by fluorescence analysis. The compounds revealed a percentage of inhibition ranging from totally inactive (0%) to almost complete inhibition (97%) (Table 1). At 50 μM, **1** and **2** showed similar inhibition (36.6 and 56.2%) but with an improvement of the percentage efficiency index (PEI) (defined as the percentage of inhibition at a given concentration/molecular weight) from 0.08 to 0.15 because of the lower molecular weight of **2** (Figure 1).

Using a novel enzyme-linked inmunosorbent assay format as a screening assay, Wang et al. found that **1** inhibited pUL89-C activity with a IC_{50} of 96 μM. These results are in a good agreement with the inhibitory response in our assay.[34]

The comparable activity of **1** and **2** corroborated our hypothesis that an α,γ-DKA scaffold linked to a 4-fluorophenyl group was the minimum motif required to modulate the UL89-C nuclease activity. We studied the importance of each individual group, α,γ-DKA and 4-fluorophenyl, in the contribution to the inhibition of the activity of UL89C by analyzing the activity of both fragments separately, **2b** and **8** (Figure S3B), and we confirmed our hypothesis that they were unable to inhibit UL89-C activity (Table 1).

On the basis of the UL89-C/**2** complex structure, several α,γ-DKA compounds decorated with different (hetero)aromatic groups spanning a wide range of size, aromaticity, and H-bond capability (**3**−**17**) were selected for further studies. The substitution of the fluorine atom of **2** for iodine (**3**) or bromine (**4**) slightly improved the activity (47.7 and 51.5%, respectively). The substitution of the methyl group of **2** for a cyclopropyl ring (**5**) showed an improvement of potency from 37.4 to 76.3%. The

DOI: 10.1021/acsomega.8b01472
ACS Omega 2018, 3, 8497−8505

improved activity of **5** might be related to the additional interaction between the cyclopropyl fragment and Phe466. Derivatization of the carboxylic acid functionality to an amide (**6** and **7**) led to inactive compounds, confirming the crucial role of the electrostatic interaction between the carboxyl group with Mn^{2+}. The replacement of the aromatic ring of **2** with a methyl (**8** and **9**, Scheme 2) resulted in a complete loss of activity as well, pointing to a possible role for the aromatic substituent in the recognition process. Altogether, these preliminary results suggested that an α,γ-DKA scaffold linked to a bulky aromatic substituent might contribute to UL89-C inhibition. Starting from this assumption, we were keen to examine the effects of different (hetero)aromatic substituents on the α,γ-DKA system. To this end, derivatives **10**−**17** (Scheme 2) were assayed. Derivatives bearing an electron-rich aromatic ring such as 4-methylphenyl (**12**), phenylpiperidine (**14**), or a heteroaromatic ring (**17**) exhibited high inhibitory activity (89.1−97.2%). Instead α,γ-DKA compounds bearing an electron-deficient aromatic ring such as a 4-fluorophenyl (**11**), 4-trifluoromethyl-phenyl (**13**), or 4-pyridyl (**15**) showed low inhibition at 50.0 μM. Structural changes introduced in the metal-chelating motif, as in **18**, greatly affected the ability of the inhibitor to bind to the active site. On top of that, the alteration of the α,γ-DKA chelating core by an α,δ-DKA (**19** and **20**) made the compounds unable to chelate the metal ions in the active site.

To estimate the IC_{50} values, the concentrations of **1**-**5**, **10**, **12**, and **14**−**17** were lowered to 25, 12.5, 6.2, and 3.1 μM, respectively, in the fluorescent UL89-C nuclease assay. At a lower concentration (25 μM), **1**−**4** showed low activity, meanwhile compound **5**, bearing a cyclopropyl group on nitrogen atom, showed the highest activity between derivatives **1**−**5**; this might be due to an additional hydrophobic interaction with Phe466. To note, the halogen atom (fluorine, iodine, or bromine) attached to the phenyl group (**2**−**4**) does influence the inhibitory potency of α,γ-DKA compounds to UL89-C. Among **10**−**17**, we observed that α,γ-DKA compounds bearing a pyridine ring (**15**), a 4-fluorobenzene (**11**), or a 4-trifluoromethyl-benzene (**13**) have low inhibitory activity against UL89-C. This might be due to the substituent effect on the electrostatic potential of the benzene ring. A strong dependence on the electrostatic potential of the aromatic ring and UL89-C affinity is suggested. Compounds bearing a benzene ring decorated with substituents such as CF_3 or F have shown to be less potent than compounds bearing electron-donating groups such as NR_2 or CH.[61,62] As expected, lowering further the concentration to 12.5 and 6.25 μM, **5**, **10**, **12**, and **16** showed a reduced percentage of inhibition (22.6−32.7%, Table 1), whereas **14** and **17** still showed good potency against UL89-C (65 and 80%, respectively). The estimated IC_{50} values for **14** and **17** are 4.5 and 9.2 μM, respectively (Figure S4A,B). Furthermore, **14** showed a PEI of 0.35, four times greater than that of **1** (PEI = 0.08, Figure 1). The high activity of **14** might be due, as predicted by docking simulation, to a strong $\pi-\pi$ interaction between Phe466 and the electron-rich aromatic ring of **14** (Figure 2D). From the focused library of α,γ-DKA, we identified that the minimal structural determinant for the UL89-C activity is an α,γ-DKA group linked to an electron-rich aromatic ring (Figure S15).

Thermal Shift Assay. Protein melting temperature (T_m) determined by thermal shift assays (TSAs) is used to monitor ligand effects on protein stability.[63] The interaction of a ligand with the protein usually causes an increase in T_m. TSA was used to study the thermal stabilization of UL89-C upon binding of **14**, **17**, and **18**, and the latter was used as a negative control (Figure 3). T_m of ligand-free UL89-C was 52.7 °C (in the presence of dimethyl sulfoxide (DMSO), T_m was 52.0 °C). A significant rise in T_m was observed for **14** (T_m = 55.7 °C) and **17** (T_m = 55.5 °C), confirming their ability to bind UL89-C and stabilizing the protein. **18** did not stabilize the protein (T_m = 52.5 °C, Figure 3), thus confirming lack of binding to UL89-C. These results further suggested that the α,γ-DKA core was a crucial motif required for UL89-C inhibition.

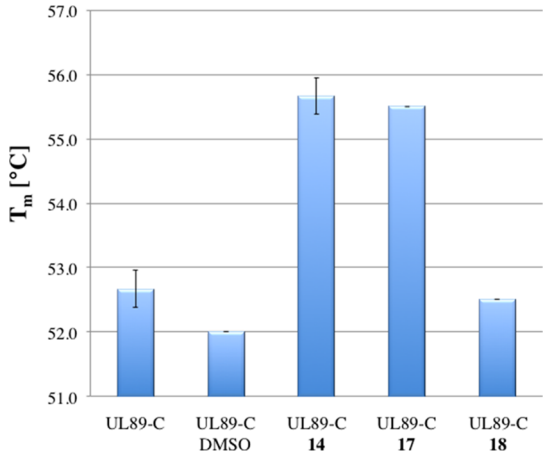

Figure 3. Thermal stability measured by TSA experiments of UL89-C/Mn^{2+} in the absence and presence of **14**, **17**, and **18** at 25 μM in DMSO. **18** was used as the negative control. Values are the mean ± standard deviation (SD) (n = 3).

Docking. Molecular docking studies were conducted to elucidate the binding mode of UL89-C inhibitors in the active site for the noncrystallized complexes. The atomic coordinates of the UL89-C active site were used for computational docking of **1**, **2**, **14**, and **17** (Figures S2A, 2D, and S2D). The binding pose of **1** showed that (i) the chelating motif was positioned close to the two Mn^{2+} cations, (ii) the 4-fluorobenzyl substituent interacted by hydrophobic interaction with Asn536 and Met579, and (iii) the oxadiazole fragment is not directly involved in the interactions with the UL89-C binding site. The predicted binding pose of **2** showed the same orientation of groups i and ii as **1**. The root-mean-square deviation (rmsd) between the docked and crystallographic poses of **2** on the UL89-C active site is 0.9 Å. Molecular docking simulation of **14** and **17** demonstrated that the α,γ-DKA group chelated the two Mn^{2+} cations and the electron-rich aromatic ring interacted with the adjacent Phe466 by $\pi-\pi$ interaction (Figures 2D and S2D).

CONCLUSIONS

UL89 HCMV terminase is a promising antiviral target because of its key role in the processing and packaging of the viral DNA inside the capsid, during viral replication. Blocking this crucial step could avoid the spread of the infection. We have focused our efforts on developing potential inhibitors against UL89-C because its nuclease activity is exclusive to the virus. On the basis of the structure of **1**, a weak inhibitor of UL89-C, we designed **2**. Compound **2**, bearing an α,γ-DKA scaffold linked to a 4-fluorophenyl group, is able to inhibit UL89-C activity. Here, we report the X-ray structure of UL89-C bound to two α,γ-DKA derivatives (**2** and **3**) as well as the in vitro thermal shift and nuclease assays. Our studies showed that the alterations of the α,γ-DKA scaffold proved to be deleterious to the activity and the

DOI: 10.1021/acsomega.8b01472
ACS Omega 2018, 3, 8497−8505

potency was influenced by substituents on the α,γ-DKA core. Among them, **14**, bearing an α,γ-DKA group linked to an aromatic electron-rich moiety, inhibited UL89-C at low micromolar range. The molecular binding of **14** to UL89-C was confirmed by a fluorescence-based thermal stability assay and its binding interactions were predicted by molecular docking simulation. Considering the strong correlation found with UL89 inhibitors against UL89 enzyme and antiviral potency,[34,35] **14** is an optimal candidate to be tested in HCMV-infected cells. Moreover, several DKA derivatives have exhibited low cytotoxicity in vitro[64−69] so we expect that **14** would share this feature in vitro as well. The structural information gained from the UL89-C/**2** complex and the identification of the chemical features determining the UL89-C inhibition will allow further development and optimization of α,γ-DKA inhibitors against the HCMV UL89-C.

EXPERIMENTAL SECTION

Synthesis of Inhibitors. Synthetic and chemical characterization for all compounds can be found in the Supporting Information General Chemistry Materials and Methods section.

X-ray Crystallography. UL89-C was purified and crystallized as previously described.[18] Crystals of UL89-C were grown by mixing the protein solution with a solution containing 10% Mes 1 M pH 6.5, 6% PEG8000, and 150 mM calcium acetate in sitting drop plates at 20 °C for 1 week. The crystal complex between the UL89-C and the inhibitor was formed by soaking the protein crystals in a solution containing 1 mM of **2** or **3**, 2 mM of $MnCl_2$, 10% Mes 1 M, 6% PEG8000, and 150 mM calcium acetate. **2** was soaked for one week, and **3** was soaked for 24 h. All crystals were cryoprotected in reservoir buffer containing 1 mM of **2** in 10% PEG400 or **3** in 20% glycerol and flash-cooled in liquid nitrogen prior to diffraction analysis. Diffraction data were recorded from cryocooled crystals (100 K) at the ALBA synchrotron in Barcelona (BL13-XALOC beamline). Data were integrated and merged using XDS[70] and scaled using XSCALE.[71] The structure of the complexes was solved by molecular replacement with the CCP4 supported program MOLREP[72,73] using the UL89-C structure (PDB code 3N4P) as a starting model and refined with Refmac[74] and manually checked with Coot.[75] **2** was placed (LigandFit, PHENIX supported program)[76] and refined (phenix.refine, PHENIX supported program)[77] in the additional electron density present at the active site pocket. For the UL89-C/**3** complex, anomalous data were collected at wavelength 0.9194 Å and the difference anomalous map was calculated (Figure S2C). Molecular topologies for **2** and **3** were generated with PRODRG server.[78] Data collection and refinement statistics are shown in Table 2.

In Vitro Nuclease Assay. Purified UL89-C at a concentration of 3 μM dissolved in a buffer containing 30 mM Tris pH 8.0 and 50 mM NaCl was mixed with 3 mM $MnCl_2$ and different concentrations of inhibitors **1**−**20** (50−3.2 μM) in DMSO. The concentration of DMSO was 5% in all reactions. The nuclease activity was started by addition of 100 ng of linear pOPINM vector, digested with KpnI−HindIII. The reaction was incubated for 30 min at 37 °C. After that time, the reaction was stopped by addition of ethylenediaminetetraacetic acid at a final concentration of 30 mM. Then, 0.2 μM of Syto 60 stain in a dye-free loading buffer was added. The samples were incubated for 10 min and loaded on an agarose gel (1%). Gel electrophoresis was run at 90 V for 45 min in the dark in 1× TAE buffer. The image of the agarose gel was obtained from the LI-COR Odyssey Infrared Imaging equipment. The non-digested DNA in the reaction was quantified using Odyssey Infrared Imaging system version 3.0 software, using a control DNA for the measurements. The percentage of inhibition was obtained from the amount of DNA present at different concentrations of inhibitors.

Table 2. Data Collection and Refinement Statistics[a]

	2-Mn^{2+}-UL89-C	3-Mn^{2+}-UL89-C
Data Collection		
wavelength (Å)	1.240	1.9997
space group	$P2_12_12_1$	$P2_12_12_1$
Unit Cell Dimensions		
a, *b*, *c* (Å)	81.6, 87.6, 186.6	81.3, 87.2, 185.3
$\alpha = \beta = \gamma$ (deg)	90	90
resolution range	30.0−2.9 (2.95−2.90)	30−4.05 (4.10−4.05)
completeness (%)	98.8 (99.7)	99.6 (100.0)
CC1/2	99.8 (65.4)	99.8 (82.5)
multiplicity	5.2 (5.6)	6.4 (6.7)
R-mean[b] (%)	8.0 (103.0)	13.5 (107.3)
I/sigma	14.4 (1.8)	10.35 (1.79)
no. of unique reflections refinement	30097 (1502)	11203 (408)
Refinement		
R_{work}[c]	0.201	
R_{free}[d]	0.239	
resolution (Å)	30−2.9	
no. reflections	30068	
Wilson plot *B*-factor	84.9	
No. of Atoms		
protein	6755	
ligand/metal ions	83	
solvent	18	
Mean *B*-Value (Å^2)		
protein	77.8	
metal ions	90.7	
ligand	100.7	
water	75.8	
rmsd Deviation from Ideal Values		
rmsd bond lengths (Å)	0.009	
rmsd bond angles (deg)	1.105	

[a]Statistic for the highest resolution shells shown in parentheses. [b]$R_{meas} = [\Sigma_h(n_h/[n_h - 1])^{1/2}\Sigma_i|\hat{I}_h - I_{h,i}|]/\Sigma_h\Sigma_i I_{h,I}$, where $\hat{I}_h = (1/n_h)\,\Sigma_i I_{h,I}$ and n_h is the number of times a reflection is measured. [c]$R_{work} = \Sigma_{hkl}||F_{obs}| - k|F_{calc}||/\Sigma_{hkl}|F_{obs}|$. [d]$R_{free} = \Sigma_{hkl\subset T}||F_{obs}| - k|F_{calc}||/\Sigma_{hkl\subset T}|F_{obs}|$ where *T* represents test set comprising ∼5% of all reflections excluded during refinement.

Thermal Shift Assay. The aliquots were prepared on ice in a 96-well polymerase chain reaction (PCR) plate (Bio-Rad) sealed with optically clear PCR sealers (Bio-Rad) and contained 15 μM UL89-C, 30 mM Tris-HCl (pH 8.0), 50 mM NaCl, Sypro Orange protein (Invitrogen), and 0.5 mM $MnCl_2$. Then, **14**, **17**, and **18** dissolved in DMSO were added at a final concentration of 25 μM. For the control, the same volume of DMSO was added to reach a final concentration of 5%. The samples were heated from 20 to 95 °C at a rate of 0.5 °C/min, and the change in fluorescence (λ_{ex} = 490 nm; λ_{em} = 575 nm) was monitored over time in an iCycler iQ Real Time PCR Detection system (Bio-Rad). All measurements were carried out in triplicate. Data evaluation and melting point determination were performed using Bio-Rad Optical System Software.

Computational Docking Studies. The 3D structures of **1**, **2**, **14**, and **17** were docked to the crystal structure of UL89-C

DOI: 10.1021/acsomega.8b01472
ACS Omega 2018, 3, 8497−8505

(PDB code: 3N4P) using AutoDock v4.2 (Molecular Graphics Lab., The Scripps Research Institute, La Jolla, CA, USA) available at http://autodock.scripps.edu. The 3D structures of **1**, **2**, **14**, **17**, and UL89-C (PDB code: 3N4P) were first converted from pdb into pdbqt format using MGL Tools. Gesteiger partial charges were used for both the enzyme and ligands. The active site was defined as a grid box centered at the −23.00, 26.75, and −4.94 coordinates with 0.4 Å units in the *x*, *y*, and *z* directions to cover the entire binding site. **1**, **2**, **14**, and **17** were docked flexibly into the active site of the UL89-C structure. Docking simulations were performed with the following parameters: number of energy evaluations (2 500 000), genetic algorithm runs (100), and population size (150).[79] The representative pose of the most populated cluster was selected.

■ ASSOCIATED CONTENT

Supporting Information

The Supporting Information is available free of charge on the ACS Publications website at DOI: 10.1021/acsomega.8b01472.

Synthetic procedures; chemical characterization for all compounds; chemical structures of HCMV terminase inhibitors; UL89-C in complex with **1**, **2**, **3**, and **17**; rational design of β,δ-DKA compounds; fragments **2b** and **8**; percentage of inhibition of UL89-C nuclease activity by **14** and **17** at different concentrations; and agarose gel image of linear DNA digested by UL89-C in the presence and absence of inhibitors (PDF)

Accession Codes

Atomic coordinates have been deposited in the Protein Data Bank under the accession code 6EY7.

■ AUTHOR INFORMATION

Corresponding Author

*E-mail: miquel.coll@irbbarcelona.org. Phone +34 93 40 34951 (M.C.).

ORCID

Salvatore Bongarzone: 0000-0002-1309-3045
Mercedes Álvarez: 0000-0002-2025-9111
Miquel Coll: 0000-0003-4471-8674

Present Addresses

[#]Division of Imaging Sciences and Biomedical Engineering, King's College London, King's Health Partners, St. Thomas' Hospital, London, SE1 7EH, United Kingdom.
[¶]Molecular Bases of Disease, Biomedical Research Institute Sant Pau (IIB Sant Pau), Barcelona 08025, Spain.
[▽]International Institute of Molecular and Cell Biology, 4 Księcia Trojdena, 02-109 Warsaw, Poland.

Author Contributions

S.B. and M.N. contributed equally and are considered co-first authors. S.B. carried out the organic synthesis, X-ray crystallography experiments, molecular docking, and nuclease assays. M.N performed protein purification and X-ray crystallography experiments. Z.K performed TSAs and crystallographic structure refinement. S.B., M.N., C.M., M.A., F.A., and M.C. analyzed the data. F.A. and M.C. conceived and supervised the project.

Notes

The authors declare no competing financial interest.

■ ACKNOWLEDGMENTS

The authors thank Jordi Juanhuix and Jordi Benach for technical assistance during data collection at Xaloc beam line at Alba Synchrotron (Barcelona, Spain). S.B. was supported by COFUND/Marie Curie fellowship (European Commission FP7). CM was supported by the RYC fellowship (grant RYC-2011-09071) from the Ministerio de Economia y Competividad (MINECO). The Institute for Research in Biomedicine Barcelona is the recipient of a Severo Ochoa Award of Excellence from MINECO. The work was partially supported by grants from the MINECO (grants BFU2011-22588, CTQ2012-30930, CTQ2015-67870P, BFU2014-53550-P, BFU2017-83720-P, Maria de Maeztu Award of Excellence MDM-2014-0435), the Generalitat de Catalunya (grants 2014 SGR 1530 and 2014 SGR 137) and the European Commission FP7 (Project SILVER-GA no. 260644).

■ REFERENCES

(1) Murphy, E.; Shenk, T. Human Cytomegalovirus Genome. In *Human Cytomegalovirus*; Shenk, T.; Stinski, M., Eds.; Springer Berlin Heidelberg, 2008; pp 1−19.
(2) Biron, K. K. Antiviral drugs for cytomegalovirus diseases. *Antiviral Res.* **2006**, *71*, 154−163.
(3) Schreiber, A.; Härter, G.; Schubert, A.; Bunjes, D.; Mertens, T.; Michel, D. Antiviral treatment of cytomegalovirus infection and resistant strains. *Expert Opin. Pharmacother.* **2009**, *10*, 191−209.
(4) Gilbert, C.; Boivin, G. Human cytomegalovirus resistance to antiviral drugs. *Antimicrob. Agents Chemother.* **2005**, *49*, 873−883.
(5) Lurain, N. S.; Chou, S. Antiviral drug resistance of human cytomegalovirus. *Clin. Microbiol. Rev.* **2010**, *23*, 689−712.
(6) De Clercq, E. Antiviral drugs in current clinical use. *J. Clin. Virol.* **2004**, *30*, 115−133.
(7) De Clercq, E. Antiviral drugs: current state of the art. *J. Clin. Virol.* **2001**, *22*, 73−89.
(8) Wathen, M. W. Non-nucleoside inhibitors of herpesviruses. *Rev. Med. Virol.* **2002**, *12*, 167−178.
(9) Andrei, G.; De Clercq, E.; Snoeck, R. Drug targets in cytomegalovirus infection. *Infect. Disord.: Drug Targets* **2009**, *9*, 201−222.
(10) Ahmed, A. Antiviral treatment of cytomegalovirus infection. *Infect. Disord.: Drug Targets* **2011**, *11*, 475−503.
(11) Castro, A.; Martinez, A. Novel agents for the treatment of human cytomegalovirus infection. *Expert Opin. Ther. Pat.* **2000**, *10*, 165−177.
(12) Martinez, A.; Castro, A.; Gil, C.; Perez, C. Recent strategies in the development of new human cytomegalovirus inhibitors. *Med. Res. Rev.* **2001**, *21*, 227−244.
(13) Härter, G.; Michel, D. Antiviral treatment of cytomegalovirus infection: an update. *Expert Opin. Pharmacother.* **2012**, *13*, 623−627.
(14) Ligat, G.; Cazal, R.; Hantz, S.; Alain, S. The human cytomegalovirus terminase complex as an antiviral target: a close-up view. *FEMS Microbiol. Rev.* **2018**, *42*, 137−145.
(15) Bogner, E. Human cytomegalovirus terminase as a target for antiviral chemotherapy. *Rev. Med. Virol.* **2002**, *12*, 115−127.
(16) Couvreux, A.; Hantz, S.; Marquant, R.; Champier, G.; Alain, S.; Morellet, N.; Bouaziz, S. Insight into the structure of the pUL89 C-terminal domain of the human cytomegalovirus terminase complex. *Proteins* **2010**, *78*, 1520−1530.
(17) Borst, E. M.; Kleine-Albers, J.; Gabaev, I.; Babic, M.; Wagner, K.; Binz, A.; Degenhardt, I.; Kalesse, M.; Jonjic, S.; Bauerfeind, R.; Messerle, M. The human cytomegalovirus UL51 protein is essential for viral genome cleavage-packaging and interacts with the terminase subunits pUL56 and pUL89. *J. Virol.* **2013**, *87*, 1720−1732.
(18) Nadal, M.; Mas, P. J.; Blanco, A. G.; Arnan, C.; Sola, M.; Hart, D. J.; Coll, M. Structure and inhibition of herpesvirus DNA packaging terminase nuclease domain. *Proc. Natl. Acad. Sci. U.S.A.* **2010**, *107*, 16078−16083.

DOI: 10.1021/acsomega.8b01472
ACS Omega 2018, 3, 8497−8505

(19) Goldner, T.; Hewlett, G.; Ettischer, N.; Ruebsamen-Schaeff, H.; Zimmermann, H.; Lischka, P. The novel anticytomegalovirus compound AIC246 (Letermovir) inhibits human cytomegalovirus replication through a specific antiviral mechanism that involves the viral terminase. *J. Virol.* **2011**, *85*, 10884−10893.
(20) Lischka, P.; Hewlett, G.; Wunberg, T.; Baumeister, J.; Paulsen, D.; Goldner, T.; Ruebsamen-Schaeff, H.; Zimmermann, H. In vitro and in vivo activities of the novel anticytomegalovirus compound AIC246. *Antimicrob. Agents Chemother.* **2010**, *54*, 1290−1297.
(21) NCT02137772. ClinicalTrials.gov Bethesda (MD): National Library of Medicine (US). 2016 Dec. MK-8228 (Letermovir) Versus Placebo in the Prevention of Clinically-Significant Cytomegalovirus (CMV) Infection in Adult, CMV-Seropositive Allogeneic Hematopoietic Stem Cell Transplant Recipients (MK-8228−001), (available from https://clinicaltrials.gov/ct2/show/study/NCT02137772, 2016).
(22) Scheffczik, H.; Savva, C. G.; Holzenburg, A.; Kolesnikova, L.; Bogner, E. The terminase subunits pUL56 and pUL89 of human cytomegalovirus are DNA-metabolizing proteins with toroidal structure. *Nucleic Acids Res.* **2002**, *30*, 1695−1703.
(23) Thoma, C.; Borst, E.; Messerle, M.; Rieger, M.; Hwang, J.-S.; Bogner, E. Identification of the Interaction Domain of the Small Terminase Subunit pUL89 with the Large Subunit pUL56 of Human Cytomegalovirus. *Biochemistry* **2006**, *45*, 8855−8863.
(24) Champier, G.; Hantz, S.; Couvreux, A.; Stuppfler, S.; Mazeron, M. C.; Bouaziz, S.; Denis, F.; Alain, S. New functional domains of human cytomegalovirus pUL89 predicted by sequence analysis and three-dimensional modelling of the catalytic site DEXDc. *Antiviral Ther.* **2007**, *12*, 217−232.
(25) Champier, G.; Couvreux, A.; Hantz, S.; Rametti, A.; Mazeron, M. C.; Bouaziz, S.; Denis, F.; Alain, S. Putative functional domains of human cytomegalovirus pUL56 involved in dimerization and benzimidazole D-ribonucleoside activity. *Antiviral Ther.* **2008**, *13*, 643−654.
(26) Visalli, R. J.; van Zeijl, M. DNA encapsidation as a target for antiherpesvirus drug therapy. *Antiviral Res.* **2003**, *59*, 73−87.
(27) Underwood, M. R.; Harvey, R. J.; Stanat, S. C.; Hemphill, M. L.; Miller, T.; Drach, J. C.; Townsend, L. B.; Biron, K. K. Inhibition of human cytomegalovirus DNA maturation by a benzimidazole ribonucleoside is mediated through the UL89 gene product. *J. Virol.* **1998**, *72*, 717−725.
(28) Krosky, P. M.; Underwood, M. R.; Turk, S. R.; Feng, K. W.; Jain, R. K.; Ptak, R. G.; Westerman, A. C.; Biron, K. K.; Townsend, L. B.; Drach, J. C. Resistance of human cytomegalovirus to benzimidazole ribonucleosides maps to two open reading frames: UL89 and UL56. *J. Virol.* **1998**, *72*, 4721−4728.
(29) Dittmer, A.; Drach, J. C.; Townsend, L. B.; Fischer, A.; Bogner, E. Interaction of the putative human cytomegalovirus portal protein pUL104 with the large terminase subunit pUL56 and its inhibition by benzimidazole-D-ribonucleosides. *J. Virol.* **2005**, *79*, 14660−14667.
(30) Underwood, M. R.; Ferris, R. G.; Selleseth, D. W.; Davis, M. G.; Drach, J. C.; Townsend, L. B.; Biron, K. K.; Boyd, F. L. Mechanism of action of the ribopyranoside benzimidazole GW275175X against human cytomegalovirus. *Antimicrob. Agents Chemother.* **2004**, *48*, 1647−1651.
(31) Williams, J. D.; Chen, J. J.; Drach, J. C.; Townsend, L. B. Design, synthesis, and antiviral activity of certain 3-substituted 2,5,6-trichloroindole nucleosides. *J. Med. Chem.* **2004**, *47*, 5753−5765.
(32) Reefschlaeger, J.; Bender, W.; Hallenberger, S.; Weber, O.; Eckenberg, P.; Goldmann, S.; Haerter, M.; Buerger, I.; Trappe, J.; Herrington, J. A.; Haebich, D.; Ruebsamen-Waigmann, H. Novel non-nucleoside inhibitors of cytomegaloviruses (BAY 38-4766): in vitro and in vivo antiviral activity and mechanism of action. *J. Antimicrob. Chemother.* **2001**, *48*, 757−767.
(33) Walker, J. E.; Saraste, M.; Runswick, M. J.; Gay, N. J. Distantly related sequences in the α- and β-subunits of ATP synthase, myosin, kinases and other ATP-requiring enzymes and a common nucleotide binding fold. *EMBO J.* **1982**, *1*, 945−951.
(34) Wang, Y.; Mao, L.; Kankanala, J.; Wang, Z.; Geraghty, R. J. Inhibition of Human Cytomegalovirus pUL89 Terminase Subunit Blocks Virus Replication and Genome Cleavage. *J. Virol.* **2017**, *91*, No. e02152-16.
(35) Wang, Y.; Tang, J.; Wang, Z.; Geraghty, R. J. Metal-chelating 3-hydroxypyrimidine-2,4-diones inhibit human cytomegalovirus pUL89 endonuclease activity and virus replication. *Antiviral Res.* **2018**, *152*, 10−17.
(36) Masaoka, T.; Zhao, H.; Hirsch, D. R.; D'Erasmo, M. P.; Meck, C.; Varnado, B.; Gupta, A.; Meyers, M. J.; Baines, J.; Beutler, J. A.; Murelli, R. P.; Tang, L.; Le Grice, S. F. J. Characterization of the C-Terminal Nuclease Domain of Herpes Simplex Virus pUL15 as a Target of Nucleotidyltransferase Inhibitors. *Biochemistry* **2016**, *55*, 809−819.
(37) Zhao, H.; Lin, Z.; Lynn, A. Y.; Varnado, B.; Beutler, J. A.; Murelli, R. P.; Le Grice, S. F.; Tang, L. Two distinct modes of metal ion binding in the nuclease active site of a viral DNA-packaging terminase: insight into the two-metal-ion catalytic mechanism. *Nucleic Acids Res.* **2015**, *43*, 11003−11016.
(38) Marchand, C.; Zhang, X.; Pais, G. C. G.; Cowansage, K.; Neamati, N.; Burke, T. R., Jr.; Pommier, Y. Structural Determinants for HIV-1 Integrase Inhibition by β-Diketo Acids. *J. Biol. Chem.* **2002**, *277*, 12596−12603.
(39) Sechi, M.; Derudas, M.; Dallocchio, R.; Dessì, A.; Bacchi, A.; Sannia, L.; Carta, F.; Palomba, M.; Ragab, O.; Chan, C.; Shoemaker, R.; Sei, S.; Dayam, R.; Neamati, N. Design and Synthesis of Novel Indole β-Diketo Acid Derivatives as HIV-1 Integrase Inhibitors. *J. Med. Chem.* **2004**, *47*, 5298−5310.
(40) Neamati, N. Patented small molecule inhibitors of HIV-1 integrase: a 10-year saga. *Expert Opin. Ther. Pat.* **2002**, *12*, 709−724.
(41) Pluymers, W.; Pais, G.; Van Maele, B.; Pannecouque, C.; Fikkert, V.; Burke, T. R., Jr.; De Clercq, E.; Witvrouw, M.; Neamati, N.; Debyser, Z. Inhibition of human immunodeficiency virus type 1 integration by diketo derivatives. *Antimicrob. Agents Chemother.* **2002**, *46*, 3292−3297.
(42) Dayam, R.; Sanchez, T.; Clement, O.; Shoemaker, R.; Sei, S.; Neamati, N. β-Diketo Acid Pharmacophore Hypothesis. 1. Discovery of a Novel Class of HIV-1 Integrase Inhibitors. *J. Med. Chem.* **2005**, *48*, 111−120.
(43) Grobler, J. A.; Stillmock, K.; Hu, B.; Witmer, M.; Felock, P.; Espeseth, A. S.; Wolfe, A.; Egbertson, M.; Bourgeois, M.; Melamed, J.; Wai, J. S.; Young, S.; Vacca, J.; Hazuda, D. J. Diketo acid inhibitor mechanism and HIV-1 integrase: implications for metal binding in the active site of phosphotransferase enzymes. *Proc. Natl. Acad. Sci. U.S.A.* **2002**, *99*, 6661−6666.
(44) Walker, M. A.; Johnson, T.; Ma, Z.; Zhang, Y.; Banville, J.; Remillard, R.; Plamondon, S.; Pendri, A.; Wong, H.; Smith, D.; Torri, A.; Samanta, H.; Lin, Z.; Deminie, C.; Terry, B.; Krystal, M.; Meanwell, N. Exploration of the diketoacid integrase inhibitor chemotype leading to the discovery of the anilide-ketoacids chemotype. *Bioorg. Med. Chem. Lett.* **2006**, *16*, 5818−5821.
(45) Walker, M. A.; Johnson, T.; Naidu, B. N.; Banville, J.; Remillard, R.; Plamondon, S.; Martel, A.; Li, C.; Torri, A.; Samanta, H.; Lin, Z.; Dicker, I.; Krystal, M.; Meanwell, N. A. Benzyl amide-ketoacid inhibitors of HIV-integrase. *Bioorg. Med. Chem. Lett.* **2007**, *17*, 4886−4890.
(46) Kirschberg, T.; Parrish, J. Metal chelators as antiviral agents. *Curr. Opin. Drug Discovery Dev.* **2007**, *10*, 460−472.
(47) Asmafiliz, N.; Kılıç, Z.; Hayvalı, Z.; Açık, L.; Hökelek, T.; Dal, H.; Öner, Y. Phosphorus−nitrogen compounds. Part 23: syntheses, structural investigations, biological activities, and DNA interactions of new N/O spirocyclotriphosphazenes. *Spectrochim. Acta, Part A* **2012**, *86*, 214−223.
(48) Barros, F. W. A.; Bezerra, D. P.; Ferreira, P. M. P.; Cavalcanti, B. C.; Silva, T. G.; Pitta, M. G. R.; de Lima, M. d. C. A.; Galdino, S. L.; Pitta, I. d. R.; Costa-Lotufo, L. V.; Moraes, M. O.; Burbano, R. R.; Guecheva, T. N.; Henriques, J. A. P.; Pessoa, C. Inhibition of DNA topoisomerase I activity and induction of apoptosis by thiazacridine derivatives. *Toxicol. Appl. Pharmacol.* **2013**, *268*, 37−46.

DOI: 10.1021/acsomega.8b01472
ACS Omega 2018, 3, 8497−8505

(49) Hare, S.; Gupta, S. S.; Valkov, E.; Engelman, A.; Cherepanov, P. Retroviral intasome assembly and inhibition of DNA strand transfer. *Nature* **2010**, *464*, 232−236.
(50) Bhatt, A.; Gurukumar, K. R.; Basu, A.; Patel, M. R.; Kaushik-Basu, N.; Talele, T. T. Synthesis and SAR optimization of diketo acid pharmacophore for HCV NS5B polymerase inhibition. *Eur. J. Med. Chem.* **2011**, *46*, 5138−5145.
(51) Shaw-Reid, C. A.; Munshi, V.; Graham, P.; Wolfe, A.; Witmer, M.; Danzeisen, R.; Olsen, D. B.; Carroll, S. S.; Embrey, M.; Wai, J. S.; Miller, M. D.; Cole, J. L.; Hazuda, D. J. Inhibition of HIV-1 ribonuclease H by a novel diketo acid, 4-[5-(benzoylamino)thien-2-yl]-2,4-dioxobutanoic acid. *J. Biol. Chem.* **2003**, *278*, 2777−2780.
(52) Summa, V.; Petrocchi, A.; Pace, P.; Matassa, V. G.; De Francesco, R.; Altamura, S.; Tomei, L.; Koch, U.; Neuner, P. Discovery of α,γ-Diketo Acids as Potent Selective and Reversible Inhibitors of Hepatitis C Virus NS5b RNA-Dependent RNA Polymerase. *J. Med. Chem.* **2004**, *47*, 14−17.
(53) Tomassini, J.; Selnick, H.; Davies, M. E.; Armstrong, M. E.; Baldwin, J.; Bourgeois, M.; Hastings, J.; Hazuda, D.; Lewis, J.; McClements, W. Inhibition of cap (m7GpppXm)-dependent endonuclease of influenza virus by 4-substituted 2,4-dioxobutanoic acid compounds. *Antimicrob. Agents Chemother.* **1994**, *38*, 2827−2837.
(54) Banville, J.; Johnson, T. D.; Meanwell, N. A.; Co, S. B. M.; Walker, M. A. HIV integrase inhibitors. WO0196283−A2, 2001.
(55) Walker, M. A.; Johnson, T. D.; Kim, O. K.; Zhang, Y. HIV integrase inhibitors. U.S. Patent 10/085,314, 2003.
(56) Zheng, S.; Thompson, J. D.; Tontcheva, A.; Khan, S. I.; Rubin, Y. Perchloro-2,5,8-triazaphenalenyl radical. *Org. Lett.* **2005**, *7*, 1861−1863.
(57) Balogh, M.; Hermecz, I.; Mészaros, Z.; Simon, K.; Pusztay, L.; Horváth, G.; Dvortsak, P. Studies on chemotherapeutics I. Synthesis of 5-substituted-4-oxo-1,4-dihydro-3-pyridinecarboxylic acid derivatives. *J. Heterocycl. Chem.* **1980**, *17*, 359−368.
(58) Ren, C.; Maurizot, V.; Zhao, H.; Shen, J.; Zhou, F.; Ong, W. Q.; Du, Z.; Zhang, K.; Su, H.; Zeng, H. Five-fold-symmetric macrocyclic aromatic pentamers: high-affinity cation recognition, ion-pair-induced columnar stacking, and nanofibrillation. *J. Am. Chem. Soc.* **2011**, *133*, 13930−13933.
(59) Reguera, J.; Weber, F.; Cusack, S. Bunyaviridae RNA polymerases (L-protein) have an N-terminal, influenza-like endonuclease domain, essential for viral cap-dependent transcription. *PLoS Pathog.* **2010**, *6*, No. e1001101.
(60) Aldrich, C.; Bertozzi, C.; Georg, G. I.; Kiessling, L.; Lindsley, C.; Liotta, D.; Merz, K. M., Jr.; Schepartz, A.; Wang, S. The Ecstasy and Agony of Assay Interference Compounds. *J. Med. Chem.* **2017**, *60*, 2165−2168.
(61) Suresh, C. H.; Gadre, S. R. Electrostatic potential minimum of the aromatic ring as a measure of substituent constant. *J. Phys. Chem. A* **2007**, *111*, 710−714.
(62) Wheeler, S. E.; Houk, K. N. Through-Space Effects of Substituents Dominate Molecular Electrostatic Potentials of Substituted Arenes. *J. Chem. Theory Comput.* **2009**, *5*, 2301−2312.
(63) Pantoliano, M. W.; Petrella, E. C.; Kwasnoski, J. D.; Lobanov, V. S.; Myslik, J.; Graf, E.; Carver, T.; Asel, E.; Springer, B. A.; Lane, P.; Salemme, F. R. High-density miniaturized thermal shift assays as a general strategy for drug discovery. *J. Biomol. Screening* **2001**, *6*, 429−440.
(64) Svarovskaia, E. S.; Barr, R.; Zhang, X.; Pais, G. C. G.; Marchand, C.; Pommier, Y.; Burke, T. R., Jr.; Pathak, V. K. Azido-containing diketo acid derivatives inhibit human immunodeficiency virus type 1 integrase in vivo and influence the frequency of deletions at two-long-terminal-repeat-circle junctions. *J. Virol.* **2004**, *78*, 3210−3222.
(65) Cuzzucoli Crucitti, G.; Métifiot, M.; Pescatori, L.; Messore, A.; Madia, V. N.; Pupo, G.; Saccoliti, F.; Scipione, L.; Tortorella, S.; Esposito, F.; Corona, A.; Cadeddu, M.; Marchand, C.; Pommier, Y.; Tramontano, E.; Costi, R.; Di Santo, R. Structure-activity relationship of pyrrolyl diketo acid derivatives as dual inhibitors of HIV-1 integrase and reverse transcriptase ribonuclease H domain. *J. Med. Chem.* **2015**, *58*, 1915−1928.
(66) Patil, S.; Kamath, S.; Sanchez, T.; Neamati, N.; Schinazi, R. F.; Buolamwini, J. K. Synthesis and biological evaluation of novel 5(H)-phenanthridin-6-ones, 5(H)-phenanthridin-6-one diketo acid, and polycyclic aromatic diketo acid analogs as new HIV-1 integrase inhibitors. *Bioorg. Med. Chem.* **2007**, *15*, 1212−1228.
(67) Pescatori, L.; Métifiot, M.; Chung, S.; Masoaka, T.; Cuzzucoli Crucitti, G.; Messore, A.; Pupo, G.; Madia, V. N.; Saccoliti, F.; Scipione, L.; Tortorella, S.; Di Leva, F. S.; Cosconati, S.; Marinelli, L.; Novellino, E.; Le Grice, S. F. J.; Pommier, Y.; Marchand, C.; Costi, R.; Di Santo, R. N-Substituted Quinolinonyl Diketo Acid Derivatives as HIV Integrase Strand Transfer Inhibitors and Their Activity against RNase H Function of Reverse Transcriptase. *J. Med. Chem.* **2015**, *58*, 4610−4623.
(68) Costi, R.; Métifiot, M.; Chung, S.; Cuzzucoli Crucitti, G.; Maddali, K.; Pescatori, L.; Messore, A.; Madia, V. N.; Pupo, G.; Scipione, L.; Tortorella, S.; Di Leva, F. S.; Cosconati, S.; Marinelli, L.; Novellino, E.; Le Grice, S. F. J.; Corona, A.; Pommier, Y.; Marchand, C.; Di Santo, R. Basic quinolinonyl diketo acid derivatives as inhibitors of HIV integrase and their activity against RNase H function of reverse transcriptase. *J. Med. Chem.* **2014**, *57*, 3223−3234.
(69) Di Santo, R.; Costi, R.; Roux, A.; Miele, G.; Crucitti, G. C.; Iacovo, A.; Rosi, F.; Lavecchia, A.; Marinelli, L.; Di Giovanni, C.; Novellino, E.; Palmisano, L.; Andreotti, M.; Amici, R.; Galluzzo, C. M.; Nencioni, L.; Palamara, A. T.; Pommier, Y.; Marchand, C. Novel quinolinonyl diketo acid derivatives as HIV-1 integrase inhibitors: design, synthesis, and biological activities. *J. Med. Chem.* **2008**, *51*, 4744−4750.
(70) Kabsch, W. XDS. *Acta Crystallogr., Sect. D: Biol. Crystallogr.* **2010**, *66*, 125−132.
(71) Kabsch, W. Integration, scaling, space-group assignment and post-refinement. *Acta Crystallogr., Sect. D: Biol. Crystallogr.* **2010**, *66*, 133−144.
(72) Vagin, A.; Teplyakov, A. MOLREP: an automated program for molecular replacement. *J. Appl. Crystallogr.* **1997**, *30*, 1022−1025.
(73) Winn, M. D.; Ballard, C. C.; Cowtan, K. D.; Dodson, E. J.; Emsley, P.; Evans, P. R.; Keegan, R. M.; Krissinel, E. B.; Leslie, A. G. W.; McCoy, A.; McNicholas, S. J.; Murshudov, G. N.; Pannu, N. S.; Potterton, E. A.; Powell, H. R.; Read, R. J.; Vagin, A.; Wilson, K. S. Overview of theCCP4 suite and current developments. *Acta Crystallogr., Sect. D: Biol. Crystallogr.* **2011**, *67*, 235−242.
(74) Murshudov, G. N.; Vagin, A. A.; Dodson, E. J. Refinement of macromolecular structures by the maximum-likelihood method. *Acta Crystallogr., Sect. D: Biol. Crystallogr.* **1997**, *53*, 240−255.
(75) Emsley, P.; Cowtan, K. Coot: model-building tools for molecular graphics. *Acta Crystallogr., Sect. D: Biol. Crystallogr.* **2004**, *60*, 2126−2132.
(76) Terwilliger, T. C.; Adams, P. D.; Moriarty, N. W.; Cohn, J. D. Ligand identification using electron-density map correlations. *Acta Crystallogr., Sect. D: Biol. Crystallogr.* **2007**, *63*, 101−107.
(77) Afonine, P. V.; Grosse-Kunstleve, R. W.; Echols, N.; Headd, J. J.; Moriarty, N. W.; Mustyakimov, M.; Terwilliger, T. C.; Urzhumtsev, A.; Zwart, P. H.; Adams, P. D. Towards automated crystallographic structure refinement withphenix.refine. *Acta Crystallogr., Sect. D: Biol. Crystallogr.* **2012**, *68*, 352−367.
(78) Schüttelkopf, A. W.; van Aalten, D. M. F. PRODRG: a tool for high-throughput crystallography of protein−ligand complexes. *Acta Crystallogr., Sect. D: Biol. Crystallogr.* **2004**, *60*, 1355−1363.
(79) Morris, G. M.; Huey, R.; Lindstrom, W.; Sanner, M. F.; Belew, R. K.; Goodsell, D. S.; Olson, A. J. AutoDock4 and AutoDockTools4: Automated docking with selective receptor flexibility. *J. Comput. Chem.* **2009**, *30*, 2785−2791.

DOI: 10.1021/acsomega.8b01472
ACS Omega 2018, 3, 8497−8505